THE ASTROPHYSICAL JOURNAL, 471:52–63, 1996 November 1

LIMITATIONS TO THE ACCURACY OF COSMIC BACKGROUND RADIATION ANISOTROPY MEASUREMENTS: ATMOSPHERIC FLUCTUATIONS

BIANCA MELCHIORRI,[1] MARCO DE PETRIS,[2] GERARDO D'ANDRETA,[2] GIANFRANCO GUARINI,[2]
FRANCESCO MELCHIORRI,[2] AND MONIQUE SIGNORE[3]
Received 1996 January 31; accepted 1996 May 9

ABSTRACT

We discuss the ultimate limits posed by atmospheric fluctuations to observations of cosmic background anisotropies (CBAs) in ground-based and balloon-borne experiments both in the radio and millimetric regions. We present correlation techniques useful in separating CBAs from atmospheric fluctuations. An experimental procedure is discussed for testing a site in view of possible CBA observations. Four sites with altitudes ranging from 0 up to 3.5 km have been tested.

Subject headings: atmospheric effects — balloons — cosmic microwave background — radio continuum: general

1. INTRODUCTION

In two previous papers (Guarini, Melchiorri, & Melchiorri 1995; Melchiorri et al. 1996) we discussed the effects of galactic dust emission in contaminating measurements of cosmic background anisotropies (CBAs). In the present work we analyze the limits posed by atmospheric fluctuations. As shown in Figure 1, atmospheric emission largely dominates over CBAs (estimated from *COBE* data to be around 30 μK at angular scales of 5°–10°) even at balloon altitude $h > 35$ km.

This picture is not very useful in planning CBA observations, however; we are much more interested in the fluctuations of the atmospheric emission rather than in its absolute flux. These fluctuations may be classified into (i) photon noise and (ii) meteorological noise. Several authors have discussed the problem of the photon noise of a gray body illuminating a bolometer (Mather 1982; Boyd 1982; Gromov 1983; Lamarre 1986), and only one attempt to detect the cosmic background radiation (CBR) noise has been reported up to now (Dall'Oglio et al. 1982). The rms amplitude of the fluctuations ΔI in the frequency region $\tilde{\nu}_1 \leq \tilde{\nu} \leq \tilde{\nu}_2$ is given by

$$\langle(\Delta I)^2\rangle^{1/2} = 2.8 \times 10^{-18} T^{5/2} \times \left\{ \int_{x_1}^{x_2} \frac{x^4 \epsilon(x)[e^x - 1 + \epsilon(x)]}{(e^x - 1)^2} dx \right\}^{1/2}, \quad (1)$$

where $T \simeq 270$ K is the mean temperature of the atmosphere; $x = h\tilde{\nu}/kT = 1.44\tilde{\nu}/T$, with $\tilde{\nu}$ the frequency in wavenumbers (cm^{-1}); $\epsilon(x)$ is the emissivity of the atmosphere and the units are in W(cm^2 sr Hz)$^{-1/2}$ (i.e., this figure is equivalent to the noise-equivalent power of a detector having a throughput (area by solid angle) $A\Omega = 1$ cm^2 sr). The limits of validity of equation (1) are determined by the condition for the number of space modes $A\Omega\tilde{\nu}^2 \geq 1$ in the case of incoherent detectors like bolometers $A\Omega \leq 1$ cm^2 sr, so that equation (1) is valid for $\tilde{\nu} \geq 1$ cm^{-1}. In the case of radio receivers, $A\Omega = \tilde{\nu}^{-2}$. The above equation can be transformed into an estimate for the minimum detectable thermodynamic temperature difference of CBR,

$$\frac{\Delta T_{\rm CBR}}{T_{\rm CBR}} = \frac{(e^{x'} - 1)}{x' e^{x'}} \frac{\langle(\Delta I)^2\rangle^{1/2}}{I_{\rm CBR}}, \quad (2)$$

where $x' = 1.44\tilde{\nu}/2.73$, and the fractional bandwidth $\Delta x/x = 2(x_2 - x_1)/(x_2 + x_1)$ is assumed to be of the order of 0.1 both for coherent and incoherent systems. In Figure 2 we have plotted the noise of a gray body with $T = 300$ K and an emissivity ranging from 0.1 down to 0.001: a few cases of measured detector noise are also plotted both for bolometers (*squares*) and radio receivers (*circles*). The numbers (1), (5), and (6) correspond to complete photometric systems already employed in searching for CBAs. The numbers (2), (3), and (4) are detector units and laboratory prototypes.

In Figure 3 we have plotted the noise expected from the atmospheric background in the case of a high mountain observatory. It is clear that in all cases except (4), the photon noise of the "gray atmosphere" is not a serious limitation.

Unfortunately, atmospheric fluctuations are expected to stay well above the previous estimates; these excesses are due to macroscopic changes in temperature, pressure, and chemical content. Depending on the mass involved, the corresponding timescales range from tens of seconds up to several hours or even days.

It is a widespread opinion that the main effect of these atmospheric fluctuations is that of increasing the overall noise of the system: this is certainly the case of long-term observations, where CBAs may be distinguished from atmospheric perturbations in terms of sidereal time. In this case, the final effect would be that of lowering the degree of confidence of any CBA detection. In balloon-borne experiments, however, and in general every time the observations are too short to point out the sporadic nature of atmospheric perturbations, one should employ different techniques to disentangle true CBAs.

Apart from satellite experiments, the simplest procedure we can imagine for taking care of atmospheric disturbance is that of removing from the analysis all the data that are too noisy: this is in fact the procedure followed in some long-term observations. It has been pointed out by Wilkinson (1994) that removing part of the data could seriously distort CBA signals, thereby affecting the final esti-

[1] Istituto di Fisica dell'Atmosfera-CNR, P.le L. Sturzo,31 I-00144 Roma, Italy.
[2] Dipartimento di Fisica, Università "La Sapienza," P.le A. Moro,2 I-00185 Roma, Italy.
[3] Ecole Normale Superieure, Lab. de Radiastronomie Millimetrique, 24 rue Lhomond, F-75231 Paris Cedex 05.

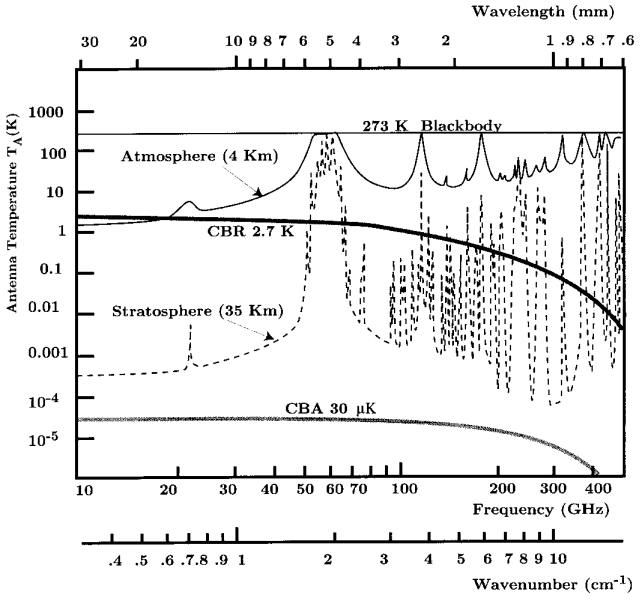

FIG. 1.—Atmospheric emission (expressed in terms of antenna temperature) vs. the frequency (wavenumber, and wavelength) for a high mountain observatory (4 km high) and for a balloon-borne experiment (35 km high). Cosmic background anisotropies at a level of 30–100 μK were reported by several authors at various angular scales (Melchiorri et al. 1981; Gaier et al. 1992; Smoot et al. 1992); their fluxes are lower than that of the atmosphere even at balloon altitude; however, their detection is not hampered by a quiet atmosphere because it is possible to disentangle them through spatial modulation.

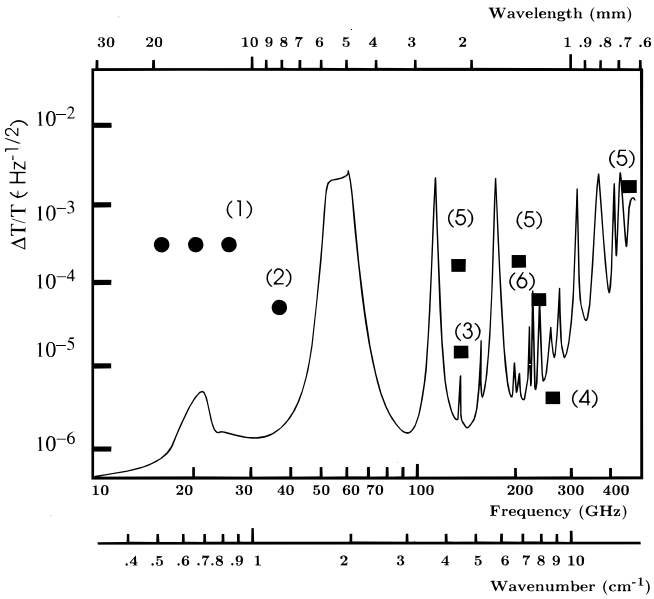

FIG. 3.—Photon noise in terms of $\Delta T/T$ as in Fig. 2, but in the case of a gray body with the same emissivity as the standard atmosphere at an altitude of about 4 km: for the explanation of the various points, see the caption of Fig. 2.

mate of the power at the given angular scale. An alternative approach is that of using several wavelengths to correct the recorded signals for the atmospheric disturbance.

Since satellite experiments are costly, time consuming, and virtually inaccessible to small research groups, we consider important to investigate the limitations posed by atmospheric disturbances very carefully: what is the minimum level of anisotropies that these disturbances allow us to detect in the case of ground-based or balloon-borne experiments?

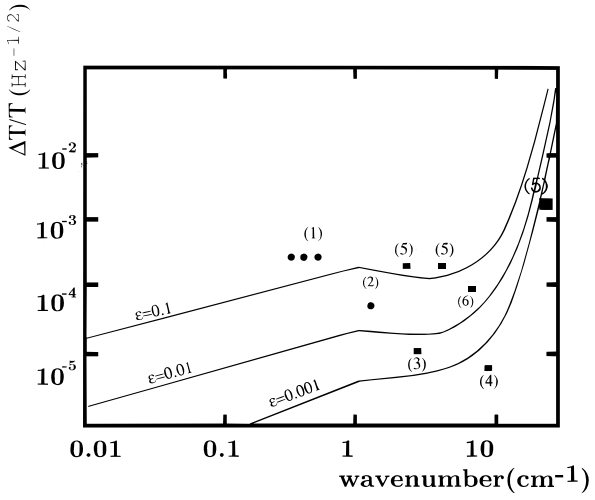

FIG. 2.—Minimum thermodynamic temperature contrast $\Delta T/T$ detectable at an electrical bandwidth of 1 Hz, in the presence of photon noise due to a gray body having a temperature of 300 K and various emissivities ϵ. The abrupt change in the lines around 1 cm^{-1} marks the difference between incoherent (*right*) and coherent (*left*) detectors. We assumed a throughput for incoherent detectors (for example, bolometers) of 1 cm^2 sr. Moreover, radio receivers are sensitive to one plane of polarization only. The points refer to (1) south pole HEMT radio receivers, (2) JPL laboratory prototype of HEMT, (3)–(4) Berkeley laboratory prototype of bolometer, (5) Microwave Anisotropy Experiment (MAX) balloon-borne bolometers, (6) ULISSE bolometer (for [1]–[5], private communication from P. Richards; for [6], see Melchiorri & Melchiorri 1992).

One of the goals of the present paper is that of fully investigating this last possibility by determining the experimental configuration for the highest correlation of atmospheric signals among the various photometric channels. We have considered the possibility that one or more of the main atmospheric components (H_2O, O_3, O_2) could fluctuate in a layer of a given thickness and at an altitude ranging from 0 to 60 km. Finally, we have investigated the conditions under which the spectral ratio of atmospheric signals among the various photometric channels could simulate the CBA spectrum. A systematic study has been carried out at different locations, such as Antarctica (sea level), Rome (sea level), Campo Imperatore (2.4 km above sea level), Testa Grigia (3.5 km above sea level), and at balloon altitude by means of eight balloon flights (ULISSE program).

2. A SIMPLIFIED APPROACH TO THE PROBLEM: THE CASE OF GROUND-BASED RADIO OBSERVATIONS

As far as we know, the first analysis of the atmospheric disturbance and its possible corrections to CBA observations was done in an unpublished NSF-CNR Proposal by Lombardini, Melchiorri, & Boynton (1974).

The main result of that analysis was that multifrequency studies can or cannot solve the problem depending on the nature of the perturbation. One should bear in mind that a real perturbation can affect one or more atmospheric components and is localized at an altitude ranging from 0 up to 60–80 km. Since the optical path is dependent on the frequency, observations at different frequencies attribute different weights to the perturbations at different altitudes: it follows that in the presence of several perturbations along the line of sight, the correlation among the various signals

may be significantly reduced unless a careful choice of frequencies is performed.

To begin with, let us assume that we are operating in the radio region ($\tilde{\nu} \leq 3$ cm^{-1} or $\nu \leq 100$ GHz), that the atmosphere is stratified in parallel layers, and that atmospheric perturbation may be represented as a small increase in the temperature or emissivity (or both) of a given layer.

The first hypothesis allows us to disregard the contribution of ozone (ozone lines are very weak in the radio region); the second hypothesis allows us to represent the atmospheric emission in terms of $T_{\rm eff}\,\epsilon(\nu)$, where $T_{\rm eff}$ is an effective temperature and $\epsilon(\nu)$ is the emissivity at the observing frequency ν averaged over the entire column path (see, for instance, the classic paper by Dicke 1946): the last hypothesis, together with the previous one, allows us to describe the disturbance as $T'_{\rm eff}\,\epsilon'(\nu)$, where both temperature and emissivity are slightly changed.

If we observe the same (not perturbed) sky region with two radiometers at the frequencies ν_1, ν_2, we expect the signals

$$S_{1,2} = T_{\rm CBR}(1 - \epsilon_{1,2}) + T_{\rm eff}\,\epsilon_{1,2}\ . \tag{3}$$

These expressions can be rearranged as

$$S_2 = T_{\rm CBR}\left(1 - \frac{\epsilon_2}{\epsilon_1}\right) + \frac{\epsilon_2}{\epsilon_1}\,S_1\ . \tag{4}$$

We can write down a similar expression for the perturbed case,

$$S'_2 = T'_{\rm CBR}\left(1 - \frac{\epsilon'_2}{\epsilon'_1}\right) + \frac{\epsilon'_2}{\epsilon'_1}\,S'_1\ , \tag{5}$$

where we have assumed that the CBR temperature is also changed slightly due to the presence of some intrinsic anisotropy. The only way to obtain $S_2 - S'_2$ independent of the atmospheric conditions is by ensuring that the ratios ϵ_2/ϵ_1 and ϵ'_2/ϵ'_1 remain equal, no matter how much the perturbations change in altitude and in chemical composition. At first glance, this appears to be a rather awkward requirement. None of the groups working in the field has attempted to solve such a problem (for a short list of experiments, see, for instance, Bersanelli et al. 1995, and references therein).

In order to investigate this question further, let us recall the expression for the absorption (or the emission) of the water vapour and oxygen (see, for instance, Rosenkranz 1975; Van Vleck & Weisskopf 1945; Ulaby 1973; Gross 1955):

$$\epsilon_{\rm O_2}(\nu) = \int_{h_0}^{\infty} \sum \left\{ \frac{\nu^2 W_{0_i} \exp\left[-\psi_i(1 - 300/T)\right]\gamma_{0_i}}{\nu_i\left[(\nu - \nu_i)^2 + \gamma_i^2(p, T)\right]} \right\} \times p^2 (300/T)^{3.89}\, dh\ , \tag{6}$$

$$\epsilon_{\rm H_2O}(\nu) = \int_{h_0}^{\infty} \sum \left\{ \frac{\nu^3 W_{0_i} \exp\left[-\psi_i(1 - 300/T)\right]\gamma_{0_i}}{(\nu^2 - \nu_i^2)^2 + 4\nu^2\gamma_i^2(p, T)} \times pp_w (300)/T)^{4.1}\, dh\ . \right. \tag{7}$$

See the references quoted above for an explanation of the various symbols. Among the quantities in braces, $\gamma_i(p, T)$ is strongly dependent on the altitude: however, if we operate at frequencies well away from the resonant one ($\nu \gg$ or $\ll \nu_i$), we can neglect γ_i^2 with respect to $(\nu - \nu_i)^2$. Finally, both γ_{0_i} and the exponent are only slightly subject to T and p. (We will return on this point later on).

In such a case, we can rewrite (with a good approximation) the total absorption as

$$\epsilon_{\rm tot}(\nu) = f(\nu)x + g(\nu)y\ , \tag{8}$$

where $f(\nu)$ and $g(\nu)$ are the sums of the terms in braces in the previous equations, and

$$x = \int_{h_0}^{\infty} p^2 (300/T)^{3.89}\, dh\ , \tag{9}$$

$$y = \int_{h_0}^{\infty} pp_w (300/T)^{4.1}\, dh\ , \tag{10}$$

It follows that in order to have ϵ_2/ϵ_1 and $\epsilon'_2/\epsilon'_1 =$ constant, one has to impose the condition

$$f(\nu_1)/g(\nu_1) = f(\nu_2/g(\nu_2) = \text{const.} \tag{11}$$

In Figure 4 we have plotted the function $\Gamma(\nu) = f(\nu)/g(\nu)$ versus ν: the choice of the operating frequencies is therefore such that $\Gamma(\nu)$ acquires the same value. The main conclusion of this analysis is that even in this simple case one has to select carefully the couple of frequencies in order to obtain a reasonable correlation. We want to stress that the choice adopted by several authors of centering one or more channels very close to resonant lines to obtain stronger atmospheric signals is not a good one: it violates the conditions under which equation (8) has been derived, and the correlation is expected to be very poor. In Figure 4 we have indicated with gray areas the zones too close to the resonant lines: a correlation greater than 90% requires us to stay outside these regions. The advantage of high-altitude observatories is evident.

Another difficulty in using the above technique lies in the fact that the field of view of a radio receiver changes with

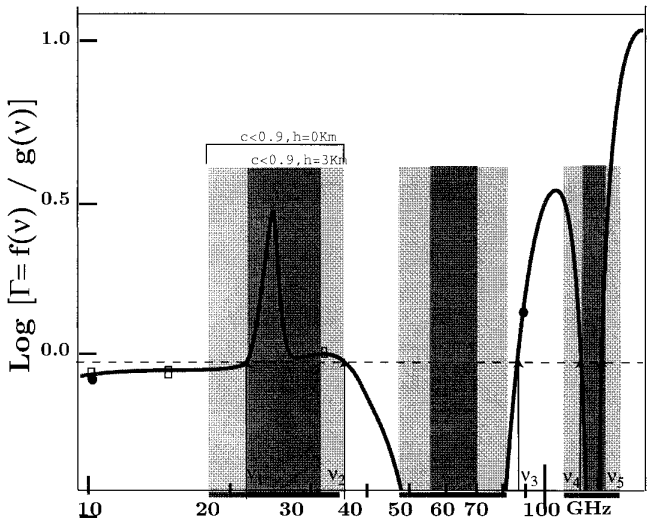

FIG. 4.—Ratio Γ of water vapor and oxygen absorption factors as given by eq. (11): an equal ratio Γ at two different frequencies provides the optimum correlation between the two radio channels. Here ν_1–ν_5 are examples of frequencies with good correlation: the frequencies selected by the Tenerife experiment (*open rectangles*) (Watson et al. 1992; Rebolo et al. 1995) or the White Mountain Collaboration (*points*) (Bersanelli et al. 1995) do not fulfil this requirement. The gray zones correspond to regions in which the correlation becomes worse than 90% even for the same values of Γ because the frequencies are too close to O_2 or H_2O resonant lines. These forbidden regions are smaller for a high mountain (4 km observatory (*darker regions*) because the line width parameter γ_{0_i} of eqs. (6)–(7) decreases as the square of the atmospheric pressure.

the frequency like $A\Omega \propto \nu^{-2}$: therefore, the outputs will be largely uncorrelated, unless the optics are designed to compensate for dependence on the wavelength. This point has been taken into consideration in the Tenerife experiment (Watson et al. 1992), in which the antennas of the three radiometers were scaled appropriately. Unfortunately, the choice of the three frequencies does not meet our requirements, and the atmospheric fluctuations are expected to be largely uncorrelated. For instance, Bersanelli et al. (1995) found a modest correlation in their 10 GHz versus 90 GHz channels as shown in Figure 4. As far as we know, none of the groups working in the radio region have selected the right frequencies for maximum correlation: on the other hand, we have to point out that the atmospheric disturbances tend to decrease as the wavelength increases toward the long-wave tail of the CBR spectrum; at frequencies lower than 30 GHz, they should represent a minor problem with respect to other contaminants like free-free and sinchrotron galactic emission.

3. THE CASE OF MILLIMETRIC GROUND-BASED OBSERVATIONS

In the case of millimetric observations, two new difficulties arise: first of all, ozone emission is no longer negligible; second, the antenna temperature $T_{\rm eff}$ employed in equation (3) becomes wavelength dependent. A third difficulty could arise from the choice of a bandwidth much larger than in the case of radio receivers; we assume $\Delta\tilde{\nu} \ll \tilde{\nu}$ for now.

Let us assume that the atmospheric emissivity is low in both channels; we can write in the case of differential measurements at two frequencies $\tilde{\nu}_1$ and $\tilde{\nu}_2$

$$\Delta S_{1,2} = \Delta I_{\rm CBR}(\tilde{\nu}_{1,2})[1 - \epsilon_{1,2}] + \Delta I_{\rm atm}(\tilde{\nu}_{1,2})\epsilon_{1,2}\,, \quad (12)$$

The problem becomes that of minimizing the quantity

$$Q = \frac{\Delta I_{\rm atm}(\tilde{\nu}_1)}{\Delta I_{\rm atm}(\tilde{\nu}_2)} - \Xi\,\frac{\epsilon_2}{\epsilon_1}\,, \quad (13)$$

and maximizing the quantity

$$W = \frac{\Delta I_{\rm CBR}(\tilde{\nu}_1)}{\Delta I_{\rm CBR}(\tilde{\nu}_2)} - \Xi\,, \quad (14)$$

where Ξ is an appropriate constant.

In order to understand this strategy better, we have studied the situation in the frequency range 4–6 $\rm cm^{-1}$ for $\tilde{\nu}_1$ and 7–9.8 $\rm cm^{-1}$ for $\tilde{\nu}_2$ (where two important atmospheric windows are present) by means of the following numerical experiment.

We divided the standard northern atmosphere into 20 layers between 0 and 20 km, applying random Gaussian fluctuations in pressure ($\Delta p \le 10^{-3} p$), in composition (O_2, O_3, $H_2O_2 \le 1\%$), and in temperature ($\Delta T \le 1\% T_A$) to each layer. We have repeated the simulation 200 times. The rms value of the atmospheric fluctuations so determined has been plotted with relation to the two selected frequencies in Figure 5.

There is an absolute minimum for Q for $\tilde{\nu}_1 \simeq 4.8$–5.2 $\rm cm^{-1}$ that corresponds to a local maximum in W.

We found that a good choice is given by $\tilde{\nu}_1 = 4.8$ $\rm cm^{-1}$ and $\tilde{\nu}_2 = 7$ $\rm cm^{-1}$. In order to test the degree of correlation between the two channels, we simulated the following experiment.

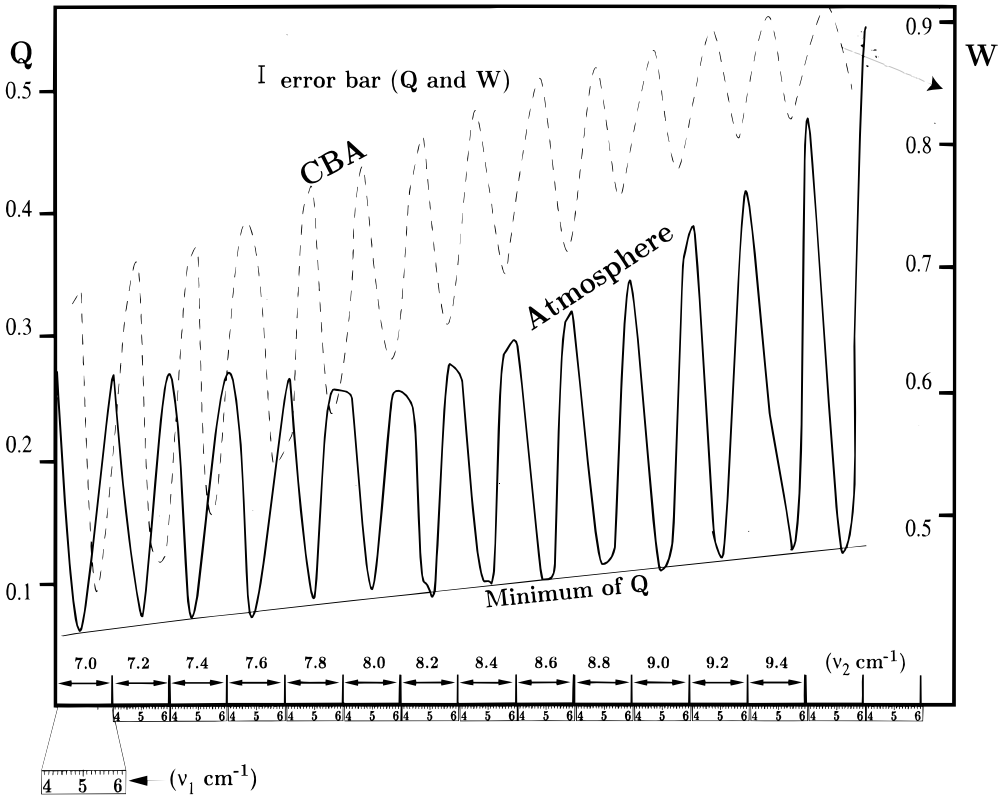

FIG. 5.—Chart for selecting the best couple of frequencies: for a given frequency in the first atmospheric window (selected within 7.0 and 9.8 $\rm cm^{-1}$ in steps of 0.2 $\rm cm^{-1}$ with a bandwidth of 0.1 $\rm cm^{-1}$ for each channel), we computed the ratio's Q (*continuous line*) and W (*dashed line*) of eqs.(13)–14), while the second frequency was changed between 4 and 6 $\rm cm^{-1}$. The absolute minimum of Q lies in the 7–7.2 $\rm cm^{-1}$ region, with the second frequency centered around 5 $\rm cm^{-1}$.

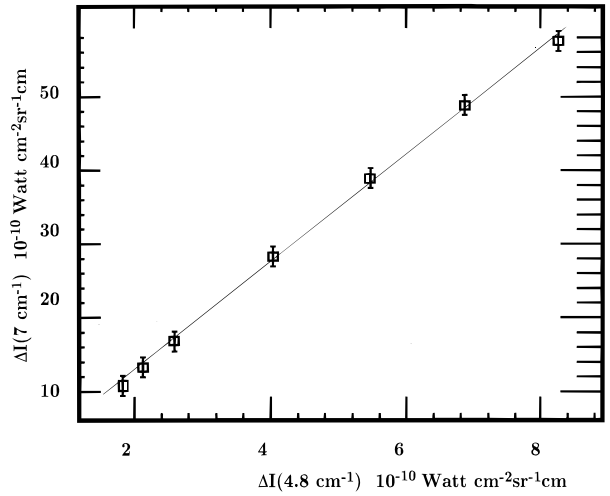

FIG. 6.—A simulated experiment of correlation for two atmospheric channels. The channels are 0.1 cm^{-1} wide and centered at the frequencies 4.8 cm^{-1} and 7.0 cm^{-1}, respectively. Atmospheric fluctuations are simulated as described in the text, and the rms value of the fluxes computed in 200 simulations are plotted. The linearity of the plot tells us that the correlation is better than 90%.

The atmosphere has been again divided into 20 layers as above. We selected two channels 0.1 cm^{-1} wide and centered at 4.8 cm^{-1} and 7 cm^{-1}. Quite arbitrary, we selected seven values of power for the 4.8 cm^{-1} channel, indicated in the abscissa of Figure 6. They correspond roughly to changes of the order of 1%–10% in composition and/or temperature of a layer located around 1–10 km of altitude. Obviously several different combinations of fluctuations and layers may produce the same amount of power on the 4.8 cm^{-1} channel. For each of the seven values, we considered 200 different combinations obtained by changing p, T, and the composition of a layer at variable altitude. Both positive and negative flux fluctuations have been considered. The corresponding power arriving on the 7 cm^{-1} channel turned out to be constrained within the vertical error bars of Figure 6. In this figure we have plotted the rms values in order to consider both positive and negative fluctuations. The linearity of the plot indicates that the correlation is better than 90%.

4. AN EXPERIMENTAL TEST OF THE CORRELATION

A test of the above model at a dry, clean site (like a high mountain observatory or in Antarctica) is rather difficult. A good site is characterized by atmospheric fluctuations comparable with the final sensitivity of the instrument; therefore, the observed signals are a mixture of these fluctuations, instrumental noise, and true sky signals (which in turn are a combination of foreground emission and CBAs). Let us consider a real experiment, such as that we are planning to carry out with MITO (Millimeter and Infrared Testagrigia Observatory). MITO consists of a 2.6 m telescope located at an altitude of 3.5 km at the Alpine Observatory of Testa Grigia (Cervinia) (De Petris et al. 1996). The photometer is a four-channel He3 system with a field of view of 17′ FWHM, and the beam is modulated up to 1° in the sky. This means that the instrument is sensitive to atmospheric perturbations with angular dimensions $5' \leq \delta\theta \leq 2°$ and located at least 1 km above the telescope.

The two basic photometric channels of MITO, called A and B, are matched with the atmospheric windows around 1.4 and 2.2 mm: their spectra are shown in Figure 7. Assuming a standard northern atmosphere, we have computed the power reaching each channel from a layer 1 km thick, located at different altitudes. We have employed the HITRAN-PC code to compute both the emission of the layer and the transmission of the atmosphere between the layer and the observer (D'Andreta, D'Addio, & Melchiorri 1995). The perturbation is simulated by increasing the abundance of H_2O, O_2, and O_3 in the layer of 1%. Figure 8 shows schematically the spectral distribution of the power on the detectors for several selected altitudes. In Figure 9 we show the power ratio Π_{atm} on the two channels B and A as a function of the altitude when all the components fluctuate (the signal is essentially due to H_2O up to 10 km and to O_3 above this altitude).

The fact that Π_{atm} is a rapidly changing function of the altitude is troublesome: if perturbations are distributed widely in altitude, we expect a poor correlation. Perturbations close to 8–12 km would show a ratio dangerously close to that of CBA (which is around 0.95): these are expected to be a tiny fraction of the total, however. More important is the fact that the ratio R,

$$R = \frac{\Delta I_{atm}(\nu_2) + \Delta I_{CBR}(\nu_2)}{\Delta I_{atm}(\nu_1) + \Delta I_{CBR}(\nu_1)}, \tag{15}$$

could fall inside the range Π_{max}–Π_{min}, so that CBAs are removed by subtraction between the two channels. If we indicate with Δ the full width of Π_{atm} distribution, we therefore require that:

$$\Delta I_{atm}(\nu_1) \leq \Delta I_{CBR} \frac{|\Pi_{CBR} - \bar{\Pi}_{atm}|}{\Pi_{max} - \Pi_{min}}$$

or

$$\Delta \leq |\Pi_{CBR} - \bar{\Pi}_{atm}| \frac{\Delta I_{CBR}}{\Delta I_{atm}}. \tag{16}$$

Therefore, the real possibility of disentangling CBAs from atmospheric fluctuations depends on the width of the

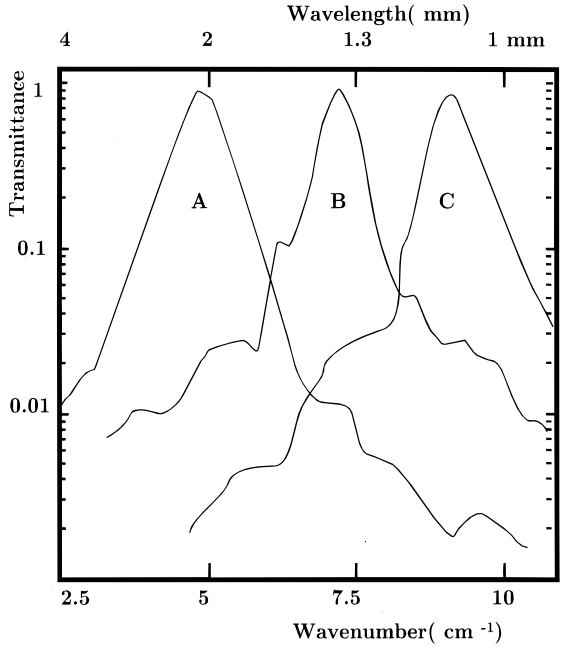

FIG. 7.—Transmittance of the three long-wavelength filters of the MITO photometer.

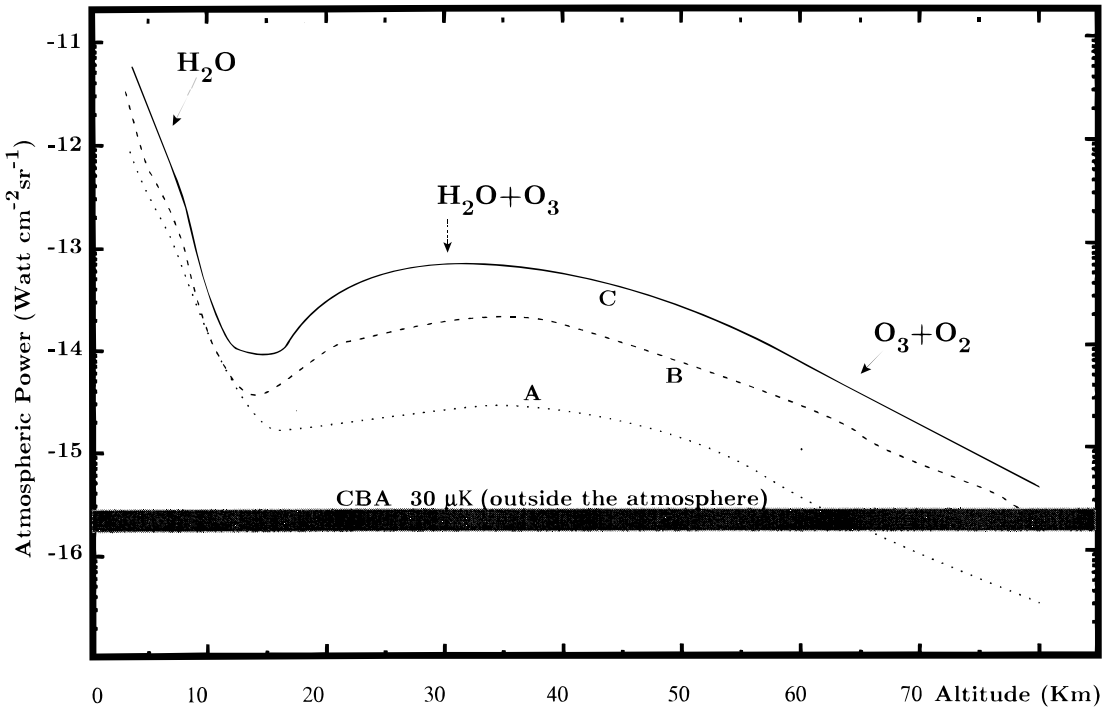

FIG. 8.—Power collected within the bandwidths of the filters A, B, and C of the previous figure and due to a layer 1 km thick located at various altitudes given in abscissa. The power is computed assuming a 1% change in composition of all the main constituents.

experimental distribution of Π_{atm} and on how far Π_{CBR} is with respect to the mean value $\bar{\Pi}_{atm}$.

Before we go any further, it is necessary to consider the problem of the intrinsic detector noise. It is clear that noise capable of increasing Δ above the limits posed by equation (16) would invalidate the efforts of disentangling CBAs from atmospheric perturbations. This means that the noise per pixel is determined by equation (16). This is quite a different situation with respect to the one usually discussed in literature for CBA observations limited by cosmic variance alone (see, for instance, Melchiorri et al. 1996). In the absence of atmospheric contamination, the best observational strategy is that of measuring the largest possible number of independent pixels with a per-pixel noise roughly $N^{1/2}$ times larger than the final signal-to-noise ratio (S/N) of CBA determined by the cosmic variance (N being the number of independent pixels). The corresponding per-pixel signal-to-noise ratio is usually smaller than unity, as in the *COBE* DMR results. In our case, we need a good per-pixel S/N in order to extract CBAs from atmospheric fluctuations; it follows that ground-based observations require much longer observational times than satellite experiments. A rough estimate of the ratio between ground-based and satellite observation times will give

$$\frac{\tau_{ground}}{\tau_{sat}} \simeq l \frac{\langle [\Delta I_{atm}(\nu_1)]^2 \rangle}{\langle (\Delta I_{CBR})^2 \rangle} \frac{1}{(\Pi_{CBR} - \bar{\Pi}_{atm})^2}, \qquad (17)$$

where l is the multipole index in spherical harmonics corresponding roughly to the inverse of the beam size.

In order to get an idea of the real situation, we decided to test it in a location in which atmospheric fluctuations are expected to be large: this choice will provide atmospheric signals well above CBA, galaxy, and detector noise. Therefore, the test has been carried out on the roof of the physics department in Rome, before transporting the telescope to Testa Grigia, during a clear, dry night in winter (the temperature was 5°C above zero, and the total water vapor content was of the order of 2 cm of precipitable water, as indicated by the meteorological military station of Ciampino Airport).

The data consist of an uninterrupted set of 1200 measurements sampled every minute with an integration time of 15 s (corresponding roughly to the time spent in each field of view due to the Earth's rotation) for a total of 20 hr. The telescope was pointing to the zenith, and the wobbling

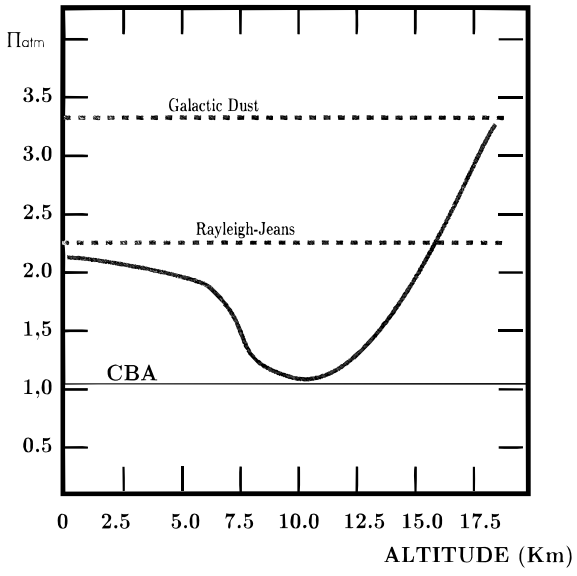

FIG. 9.—Ratio of the signals expected in channel B over channel A (see Fig. 7 for the transmittances) in relation to the altitude of the atmospheric layer perturbed by 1% in composition. The ratios due to galactic dust, CBAs, and diffused RJ Earth's radiation are also shown. We want to stress that an atmospheric disturbance around 8–12 km would produce signals in the two photometric channels dangerously close to the CBA ratio.

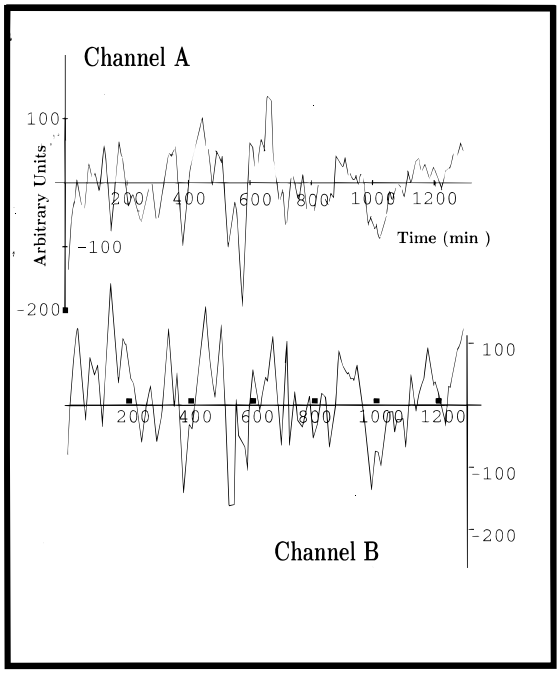

FIG. 10.—Test of correlation carried out on top of the building of the physics department of Rome University during a clear cold day and night in winter. The noise of the two channels was around 5 mK rms in 1 s of integration.

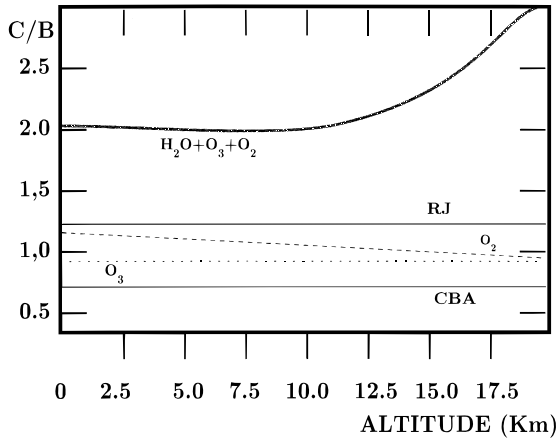

FIG. 12.—Signals ratio as in Fig. 9 but in the case of channels C and B. Note that now the ratio is much less dependent on the altitude and significantly different from CBA.

amplitude was $\pm 0.^{\circ}5$ in the sky. The raw synchronous demodulated data are shown in Figure 10 before any manipulation. The large negative signal around $t \simeq 600$ minutes was due to a visible cloud crossing the field of view

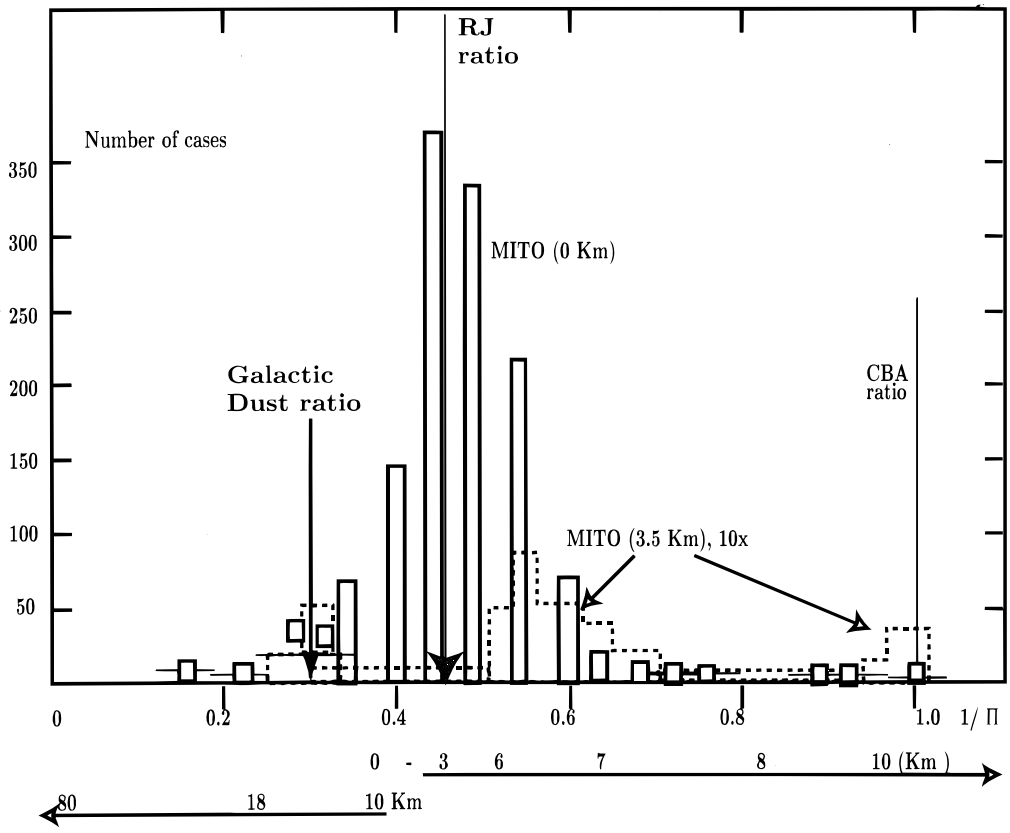

FIG. 11.—Histogram of the A/B ratios in the case of observations carried out in Rome and preliminary observations at MITO with the french two-channel "Diabolo" (*dashed line*) (Benoit et al. 1996). We note that the bulk of the atmospheric fluctuations are due to perturbations located within 5 km above the instrument. On the basis of relations (15)–(16) it is impossible to extract CBAs from the data of the Rome experiment, while it is possible at 3.5 km of altitude (Testa Grigia Observatory) if atmospheric perturbations are not larger than 10 times CBA. Note that some hint of having observed true CBAs at Testa Grigia is suggested by the presence of a small number of signals with A/B $\simeq$ 1.

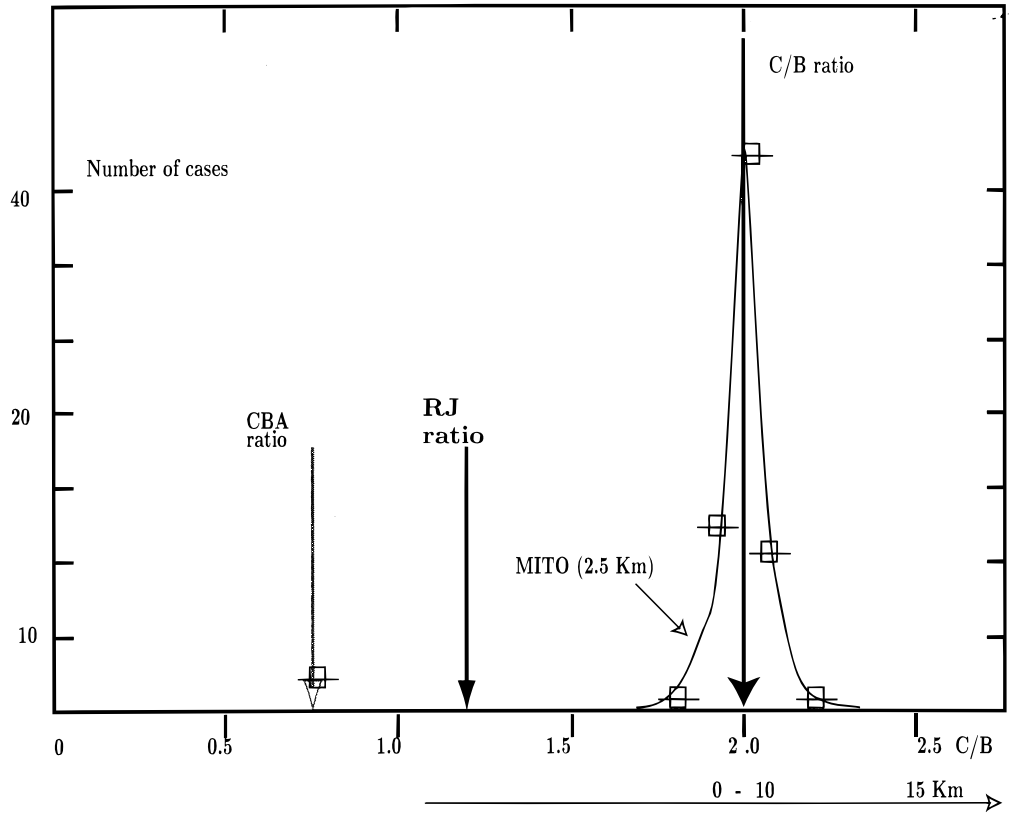

FIG. 13.—The same statistics as in Fig. 11, but for C and B filters. The observations have been carried out at the mountain station of Campo Imperatore, 2.5 km above sea level. The distribution is sharper, and it appears possible to disentangle CBAs from the atmosphere even if the last produces signals 20 times more intense than CBAs.

of the "negative" beam. In order to establish the correct ratio between the two signals, we observed the Moon. A Rayleigh-Jeans (RJ) source would produce a ratio around $\Pi = 0.45 \pm 0.05$ in which the uncertainty is due to the photometric accuracy of the filter spectra as well as to the uncertainty introduced by the correction for the atmospheric absorption; the last one was estimated by wobbling the secondary mirror perpendicularly to the horizon and measuring the secant law for the gradients of atmospheric emission. Only the signals more than 3 σ above the detector noise were used to compute Π in order to avoid too much dispersion in the ratio between the two channels. The Π statistics is shown in Figure 11, where we have plotted the number of independent measurements with the ratio $\Pi^{-1} = \Delta I_A/\Delta I_B$ as given in abscissa. We note that the distribution peaks around the RJ value, which corresponds to an altitude between 0 and 5 km. It is not surprising that the bulk of the perturbations are concentrated in this zone. The distribution decreases more rapidly on the left side, and this fact is also in qualitative agreement with the results of Figure 8: only very high altitude perturbation can contribute to these low values of Π^{-1}. Taking $\Pi_{\rm atm}^{-1} \simeq 0.45\ \Pi_{\rm CBR}^{-1} \simeq 1$ and $\Delta \simeq 0.2$ from Figure 11, equation (16) tells us that atmospheric fluctuations in channel A can be removed if they are no more than 6 times greater than CBA. Unfortunately, the observed fluctuations were at least 20 times larger than the expected CBA: The first firm conclusion is that we cannot remove atmospheric disturbances from the data by means of the outlined correlation technique: CBA observations are impossible from the roof of the Rome Physics Department!

Two facts contribute to this failure:

1. The A/B ratio is strongly dependent on the altitude, as shown in Figure 9; and
2. The perturbations are in fact broadly distributed in altitude.

Since the A and B channels match the atmospheric windows, before changing them, one should investigate point (2) in the case of a mountain observatory. As a matter of fact Figure 11 shows that the bulk of the perturbations are concentrated below 5 km, and one could anticipate different statistics for a site like Testa Grigia. Unfortunately, $\Pi_{\rm min}$ decreases with altitude up to 10 km, where it approaches $\Pi_{\rm CBR}$: if we do not expect a substantial change in Δ, the only possibility of extracting CBAs from the data is if the atmosphere becomes so quiet so as to have fluctuations comparable with CBAs within the limits posed by equation (16). Preliminary tests at Testa Grigia are shown as a broken line in Figure 11 (Benoit et al. 1996).

Although the statistics is much more modest (only 1 hour of data), it follows that CBAs can be separated from atmospheric perturbations if the latter are no more than 10 times bigger; such a situation seems to occur during clean cold nights (several hours satisfying this requirement were found from 2 to 5 A.M. local time in the month of 1995 March with an atmospheric noise below 0.1 mK rms).

If we want to improve the situation, we are forced to change the channels to obtain a slower dependence of Π on the altitude.

In the four-channel photometer devoted to MITO, a third channel at 1.1 mm is available: see the transmittance

curve C in Figure 7. The C/B ratio is shown in Figure 12, where also we have plotted the estimates for CBA, galactic dust, and RJ ratios.

We note that C/B ratio is less sensitive to the location of the perturbations and not too different for 0_3 and O_2. We are currently testing the Π statistics for this new configuration. In Figure 13 we have plotted results obtained at the mountain observatory of Campo Imperatore, 2.5 km above sea level. We note that the distribution is concentrated around the value C/B $\simeq 2$ well away from the CBA ratio. By using constraints (15) and (16), it is possible to say that CBA signals may be extracted from data if atmospheric disturbances are not larger than about 20 times CBA. In conclusion, multifrequency correlation techniques may help in removing atmospheric noise from CBA data, but the rejection can hardly exceed a factor of 10. Sites for CBA observations must be selected carefully in order to minimize atmospheric disturbances. Figures 11 and 13 together with equation (16) offer the best criteria of selection.

5. BALLOON-BORNE EXPERIMENTS

Time after time we find claims of "stratospheric disturbances" observed by groups involved in far-infrared balloon experiments. While it is now clear that some of these claims were false and the observed signals can be explained in terms of instrumental artifacts, a detailed analysis of a series of 10 balloon flights in the framework of the so-called ULISSE program has led to the observation of stratospheric disturbances (Melchiorri & Melchiorri 1995). Here again the technique of correlation between two photometric channels has shown the presence of at least two different kinds of perturbations (see Fig. 14). A first kind of perturbation has the spectral ratio as expected for a temperature or global density fluctuation in a localized sky region, while a second one seems to show a dust-like spectrum. All these perturbations have large-scale patterns, and there is no evidence for small-scale perturbations below 1°. Melchiorri & Melchiorri (1995) have attempted to classify them as a link between ionospheric traveling disturbances (well known to radio and radar technicians) and noctilucent clouds observable at high latitudes in the visible.

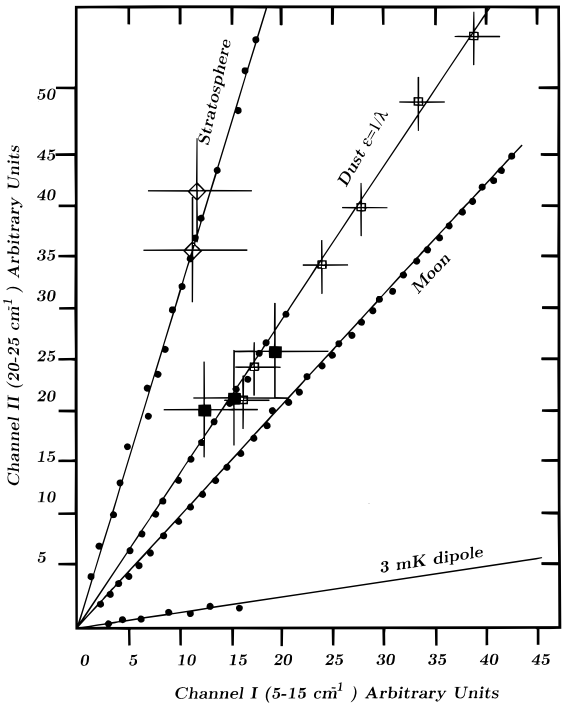

FIG. 14.—Signals measured at balloon altitude in two photometric channels with the frequencies and bandwidths (half-maximum) as specified. We note the different ratios in the cases of the Moon, CBA dipole, galactic dust, and stratosphere, which allowed us to disentangle the various contributions (see text for a discussion) (Melchiorri & Melchiorri 1995).

Figure 15 shows the distribution of the ratio between two photometric channels centered around the spectral regions 5–15 cm^{-1} and 20–25 cm^{-1}, respectively. Observations of the Moon have been used to establish the RJ ratio; observations of dipole anisotropy gradients have provided $\Pi_{\rm CBA}$. Measurements of the galactic dust emission have provided $\Pi_{\rm dust}$. Finally, stratospheric gradients have been measured by tilting the direction of modulation with respect to the horizon. All these measurements are plotted as points in Figure 14, and the relative error bars are omitted for clarity.

The filled squares, open squares, and open diamonds refer to different balloon flights: the "local" origin of these signals is proved by their duration, much shorter than the total observing time spent on the same sky region.

Since the stratosphere seems to have quite a stable emission and its perturbations have well-defined spectral properties, one could raise the question, is it possible to cancel both the perturbations and galactic signals simultaneously, through an appropriate choice of a couple of frequencies? For instance, let us assume that the two photometric channels are chosen as follows:

Channel A: from 3 cm^{-1} to a cutoff frequency $v_{\rm ct}$;

Channel B: centered around a frequency $v_B = kv_{\rm ct}$ with a bandwidth of about $0.1v_B$, where k is a suitable constant to be determined. Both k and $v_{\rm ct}$ are selected in such a way as to obtain

$$\frac{\Delta I_{\rm atm}(B)}{\Delta I_{\rm atm}(A)} \simeq \frac{\Delta I_{\rm gal}(B)}{\Delta I_{\rm gal}(A)} \simeq \frac{\Delta I_{\rm RJ}(B)}{\Delta I_{\rm RJ}(A)}\,, \tag{18}$$

where "atm" stands for atmospheric emission, "gal" stands for galactic emission, and "RJ" stands for Rayleigh-Jeans emission, the latter being due to the Earth's radiation diffused into the line of sight. In Figure 16 we have plotted the B/A ratios of the above equation as expected in the two cases $k = 1.2$ and $k = 1.6$ as a function of the cutoff frequency $v_{\rm ct}$. We can see that the three curves are very close to each other for $k = 1.6$ and $v_{\rm ct} \simeq 30$ cm^{-1}. This situation led us to test the correlation in the course of five balloon experiments carried out between 1978 and 1990. The points plotted in Figure 16 correspond to the ratio observed, while the stratospheric emission was modulated by tilting the wobbling angle of the optical system, or when a high-latitude dust cloud (L134) was crossing the field of view and, finally, when the Moon was in the field of view. All are close to 0.8. Therefore, we selected $K = 1.6$ and $v_{\rm ct} = 28$ cm^{-1}. The experiment has been described already by de Bernardis et al. (1992), and it was possible to remove all the foregrounds by more than a factor 10. The residuals have been interpreted by de Bernardis et al. (1992) as upper limits to CBA (35 μK rms at the angular scale of 6°).

In Figure 17 we have shown the map of a sky region explored by the ULISSE program co-adding the data of five balloon flights: the map has been completed by filling the uncovered regions by means of a kringing technique (Transform, Spyglass software). For comparison, the first

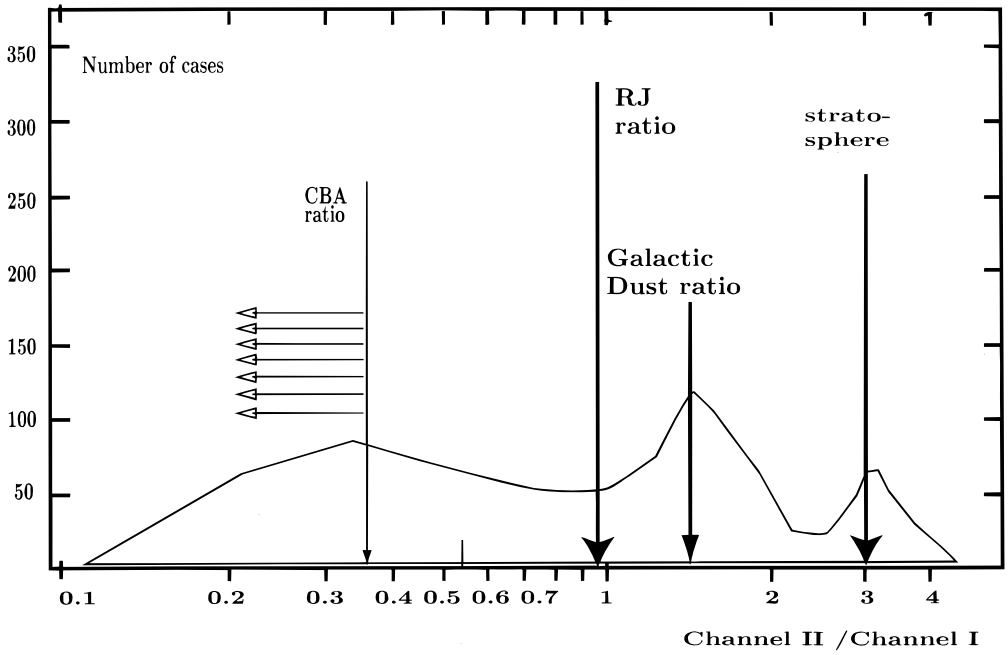

FIG. 15.—Statistics as in Figs. 11 and 13 in the case of the ULISSE program (10 balloon flights). Note that CBA signals are expected to be very small in channel II: therefore, we have considered as possible CBA detections the cases with the signal in channel I larger than 3 σ and the ratio channel II/channel I ≤ 0.3.

map has been obtained from *IRAS* data at 100 μm, where the beam has been smoothed with the ULISSE beam (Gaussian with 6° at FWHM), the *IRAS* data corresponding to uncovered pixels have been removed, and the same procedure of kringing has been applied to the data. Note that residual signals are at 1–3 σ above the detector noise. The similarity in amplitude with *COBE* DMR results may suggest that real CBA signals have been observed. An analysis of ULISSE-*COBE* data correlation will be published elsewhere. The main conclusion of this analysis is that it is possible to remove the bulk of foreground radiation and extract cosmological signals even from data taken with instruments having a very large bandwidth, if the cutoff frequency is chosen appropriately.

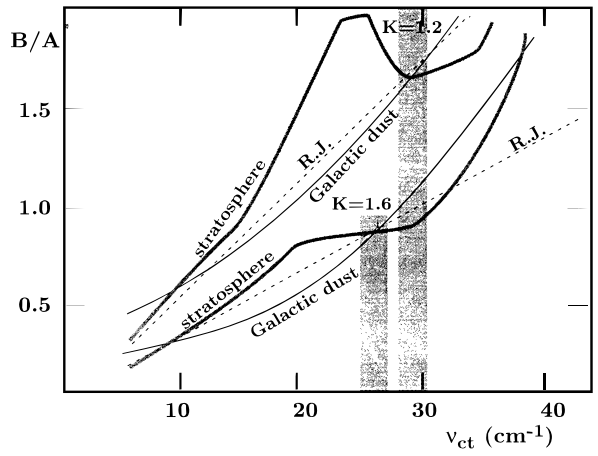

FIG. 16.—Signal ratios between the two channels of eq. (18) as a function of the cutoff frequency, as explained in the text. The shaded regions indicate the zones of maximum correlation for atmospheric, galactic, and RJ signals. The experimental points have been obtained during the ULISSE balloon flight of 1980.

6. CONCLUSIONS

The choice of the observation platform is one of the main unsolved questions in observational cosmology: high mountain, South Pole, airborne, balloon-borne, or satellite. Each choice has its advantages and disadvantages. If galactic contamination (dust, free-free) is small, there is no doubt that satellite experiments offer a significant advantage in terms of total observation time with respect to ground-based experiments, as indicated by equation (17). On the other hand, if galactic contamination is severe, the same procedure employed for correcting atmospheric fluctuations is needed, and the choice of a satellite experiment becomes much less attractive. In two previous papers, we have shown that this could well be the case (Guarini et al. 1995; Melchiorri et al. (1996).

Given the preferred or expected ratio $\Delta T/T$ of CBAs, high mountain observations through the atmospheric windows at 3.2, and 1 mm are possible if atmospheric fluctuations are not larger than 20 times the expected CBA: this goal is obtained by a careful selection of the bandwidths. During the first month of observations at MITO, we had 20 days with atmospheric noise below 20 μK rms at night. This means that the goal of 1 μK rms with an angular resolution $\leq 10'$ is within the range of possibilities of a high mountain observatory.

It is widely believed that balloon-borne observations must be carried out at 2 or 3 mm with a bandwidth as small as possible in order to minimize the contamination by galactic dust and/or stratospheric disturbances. This has led several groups to develop very low temperature systems which in turn are fragile and easily subject to damage. Our

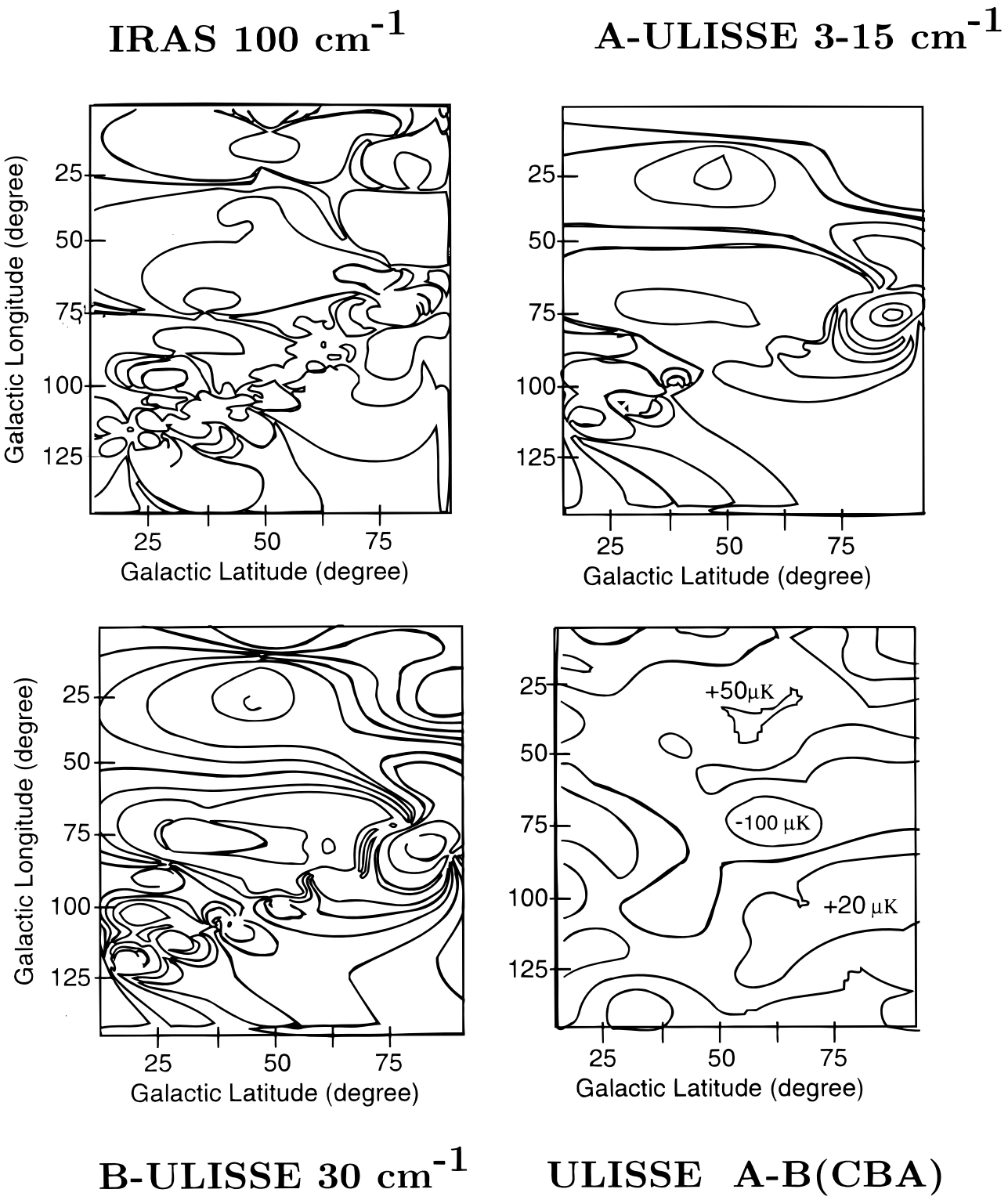

FIG. 17.—Example of the possibility of removing both the galactic and atmospheric background. The *IRAS* 100 μm smoothed map has been obtained with the same technique employed to build up the two A and B maps from Ulisse data (see text). Subtraction of B from A has left signals ranging from -100 and $+60$ μK up to 3 σ above the detector noise. Isophotes of *IRAS* map are within $\pm$ 5 MJ sr^{-1}; in the case of ULISSE, antenna temperatures are $\pm$ 0.6 mK; For ULISSE-B, antenna temperatures are $\pm$ 0.5 mK, and in the case of ULISSE A-B thermodynamic temperatures are $\pm$ 0.1 mK. The residuals correspond to 35 μK rms. They have been considered as an upper limit to CBAs before *COBE* DMR observations at the same angular scale (de Bernardis et al. 1992).

results suggest that is possible to remove galactic and stratospheric fluctuations at a level at least comparable with CBAs even in the case of a bandwidth extending from 3 to 15 cm^{-1} when a careful choice of the second channel allows for a complete cancellation of residual galactic emission. There is no evidence for stratospheric disturbances at angular scales smaller than 1°–5°.

This work has been supported by Italian MURST 40% and 60% funds.

REFERENCES

Benoit, A., et al. 1996, in preparation
Bersanelli, M., et al. 1995, ApJ, 448, 8
Boyd, R. W. 1982, Infrared Phys., 22, 157
Dall'Oglio, G., de Bernardis, P., Masi, S., & Melchiorri, F. 1982, in IAU Symp. 104, Early Evolution of the Universe and Its present Structure, ed. G. O. Abell & G. Chincarini (Dordrecht: Reidel), 135
D'Andreta, G., D'Addio, L., & Melchiorri, B. 1995, Infrared Phys. Technol., 36, 955
de Bernardis, P., Masi, S., Melchiorri, F., Melchiorri, B., & Vittorio, N. 1992, ApJ, 397, L57
De Petris, M., et al. 1996, New Astron., in press
Dicke, R. H. 1946, Rev. Sci. Instrum., 17, 268
Gaier, T., et al. 1992, ApJ, 398, L1
Gromov, V. D. 1983, IKI (Academy of Science of USSR) Internal Note 784
Gross, E. P. 1955, Phys. Rev., 97, 395
Guarini, G., Melchiorri, B., & Melchiorri, F. 1995, ApJ, 442, 23
Lamarre, J. M. 1986, Appl. Opt., 25, 870
Lombardini, P., Melchiorri, F., & Boynton, P. 1974, CNR-NSF Proposal, unpublished
Mather, J. C. 1982, Appl. Opt., 21, 1125
Melchiorri, B., & Melchiorri, F. 1992, in Current Topics in Astrofundamental Physics, ed. N. Sanchez & A. Zichichi (Singapore: World Scientific), 148
———. 1995, Infrared Phys. 36, 893
Melchiorri, F., Guarini, G., Melchiorri, B., & Signore, M. 1996, ApJ, 464, 18
Melchiorri, F., Melchiorri, B., Ceccarelli, C., & Pietranera, L. 1981, ApJ, 250, L1
Rebolo, R., Watson, R. A., Gutierrez de la Cruz, C. M., Davies, R. D., Lasenby, A. N., & Hancock, S., 1995, Astrophys. Lett. Commun., 32, 211
Rosenkranz, P. W. 1975, IEEE Trans. Ant. Prop., AP-23, 498
Smoot, G. F., et al. 1992, ApJ, 396, L1
Ulaby, F. T. 1973, IEEE. Trans. Ant. Prop., 12, 266
Van Vleck, J. H., & Weisskopf, V. F. 1945, Rev. Mod. Phys., 17, 227
Watson, R. A., et al. 1992, Nature, 357, 660
Wilkinson, D. T. 1994, presented at annual meetings of Lake Louise Winter Institute, February